Hindawi
Journal of Nanomaterials
Volume 2024, Article ID 8813109, 16 pages
https://doi.org/10.1155/2024/8813109

Research Article

Catalytic Degradation Efficacy of Silver Nanoparticles Fabricated Using *Actinidia deliciosa* Peel Extract

Maya Kassem Agha,[1] Batoul Maatouk ,[2] Rami Mhanna ,[2] and Mohammad H. El-Dakdouki [1]

[1]*Department of Chemistry, Faculty of Science, Beirut Arab University, P.O. Box 11-5020, Riad El Solh, Beirut 11072809, Lebanon*
[2]*Department of Biomedical Engineering, Faculty of Engineering and Architecture, American University of Beirut, P.O. Box 11-0236, Riad El-Solh, 1107 2020, Beirut, Lebanon*

Correspondence should be addressed to Mohammad H. El-Dakdouki; m.eldakdouki@bau.edu.lb

Received 31 August 2023; Revised 12 March 2024; Accepted 14 March 2024; Published 9 April 2024

Academic Editor: Antonio Vassallo

The preparation of metallic nanoparticles using green synthetic approaches and its application toward the efficient degradation of environmentally hazardous dyes constitutes an attractive alternative to currently employed methods. In the current report, the green synthesis of silver nanoparticles (AgNPs) was successfully achieved using *Actinidia deliciosa* (kiwifruit) peel aqueous extract as a bioreducing agent under optimized synthesis conditions. The experimental parameters were optimized in terms of reactant ratio, reaction temperature, and reaction time. The biogenic nanoparticles exhibited SPR absorption band at λ_{max} 480 nm. Transmission electron microscopy (TEM) and scanning electron microscopy (SEM) images revealed quasispherical monodisperse nanoparticles which were 36 nm in diameter. The hydrodynamic diameter of the nanoparticles was 106 nm as determined by dynamic light scattering, and the highly negative ζ-potential (−34 mV) supported its superior colloidal stability. Energy dispersive X-ray confirmed that silver is a major constituent of the nanoparticles. X-ray diffraction (XRD) diffractograms confirmed the crystallinity of the nanoparticles and its face-centered cubic (*fcc*) lattice structure. The functional groups in the plant's phytochemicals facilitating the reduction of Ag^+ ions and stabilization of the formed AgNPs were identified by fourier transform infrared (FTIR) spectroscopy. In specific, the bands in the FTIR spectra at 3,412, 1,618, 1,419, and 1,237 cm^{-1} suggested the presence of phenolic compounds. Phytochemical analysis by colorimetric assays revealed that the kiwifruit peel extract was rich in phenolic compounds. When evaluated in the catalytic degradation of organic dyes, the biosynthesized AgNPs induced instant and complete discoloration of the methylene blue dye when 1.6 mg of nanoparticles was used. At a lower dose of AgNPs (0.4 mg), 80% degradation of the dye occurred after 3 hr of treatment. The degradation reaction followed second-order kinetics with a rate constant of 0.01083 $mM^{-1}s^{-1}$. The current study highlights the immense potential of the prepared nanoparticles as efficient catalysts for the degradation of hazardous organic dyes such as methylene blue and presents an intriguing argument for investigating the catalytic efficiency of the biogenic AgNPs for the degradation of other structurally different dye pollutants.

1. Introduction

Metallic nanoparticles have found a broad spectrum of applications in numerous sectors of industry [1–8]. In specific, silver nanoparticles received immense renewed interest because of their characteristic physical and chemical properties and the broad spectrum of applications in various facets of biomedical and environmental fields. In fact, AgNPs hold several advantages over other noble metals including low cost, biocompatibility, high electrical and thermal conductivity, catalytic activity, nonlinear optical behavior, and antimicrobial activity against various strains of microbes including bacteria and fungi [9]. Because of these unconventional attributes and many others, AgNPs account for more than half of the nanoparticles utilized in commercial products in the market [10].

Traditionally, AgNPs were synthesized using different physical and chemical methods. Physical methods, which include, among others, thermal evaporation, electrolysis, ultrasonication, laser ablation, and high-energy ball milling, are limited by the high operational cost and energy demand, as well as the use of expensive sophisticated equipment [11, 12]. On the other hand, chemical methods which rely on the reduction of silver salts using reducing agents such as hydrazine and sodium borohydride are limited by the hazardous nature of the reductants and

the associated by-products. Furthermore, stabilizing capping agents are required to prevent agglomeration and clustering of the nanoparticles upon their formation. In this regard, green nanotechnology presents a biorenewable, cheap, and environmentally benign approach for the preparation of nanoparticles in general, and AgNPs in particular [13].

Green synthetic methods of nanoparticles use nontoxic biomaterials (polysaccharides, vitamins, amino acids, etc.), enzymes, microwaves, as well as biological methods that are immensely becoming popular for nanoparticles synthesis. Biological methods for the orchestration of nanoparticles can be broadly categorized into microbial-based (using various forms of microorganisms such as algae, fungi, yeast, bacteria, and viruses) and plant mediated [14]. Many plants, as a whole or their roots, leaves, fruit, or peels, were used in the green preparation of AgNPs [15]. For example, the flower of *Acmella oleracea* [16], the fruit of *Prunus serotina* [17], the leaves of *Teucrium polium* [18], the leaf gel of *aloe vera* [19], the seed of *Artocarpus heterophyllus* [20], and roots of *Chelidonium majus* [21] were used for the biosynthesis of AgNPs. The richness of the plant extracts in phytochemicals with high reducing potential such as phenolic compounds, terpenoids, flavones, alkaloids, and polysaccharides, rendered them ideal for the fast, energy-efficient, and high yield fabrication of nanoparticles. In addition to their availability in nature, plants are considered an environmentally benign nontoxic source of reducing agents whose handling and application in the biogenic synthesis of nanoparticles does not require special technologies or instrumentation. Furthermore, plants' phytochemicals exhibit the dual function of reducing the metal salts into nanoparticles as well as act as capping agents to stabilize the prepared nanoparticles and prevent agglomeration.

Recently, there has been increasing awareness and directed strategies toward recycling rejected materials in general and agricultural waste in specific for various applications such as energy recovery and production of organic fertilizers [22]. One of the agro-waste that has been utilized in the biosynthesis of nanoparticles is the kiwifruit (*Actinidia deliciosa*) peels that are rich in polyphenols and other antioxidants. In fact, the peels of kiwifruit have been employed in the biofabrication of several nanoparticles, such as zinc oxide, titanium oxide, and tin oxide nanoparticles [23]. Therefore, the aim of the current investigation is to assess the utility of the aqueous extract of kiwifruit peels as a bioreducing and capping agent for the biogenic synthesis of AgNPs. The reaction parameters were optimized, and the prepared nanoparticles were comprehensively characterized by diverse analytical techniques. Phytochemical analysis was performed to evaluate the efficiency of the extract as a potential green-reducing agent. In addition, the environmental benefits of the biosynthesized AgNPs will be evaluated in the degradation of methylene blue, a heterocyclic azo dye used in the textile industry, and is reported to be toxic and carcinogenic, posing several risks to human health. In addition, the direct release of the dye into water bodies would lead to oxygen depletion and thus adversely impact aquatic life [24].

2. Experimental Part

2.1. Materials. Kiwifruits were purchased from local grocery stores in Tripoli, Lebanon. Silver nitrate ($AgNO_3$)-99.9% pure was obtained from Scott Sciences, UK. Folin–Ciocalteu, sodium borohydride ($NaBH_4$), sodium nitrite ($NaNO_2$), and ethanol were purchased from Sigma–Aldrich. Sodium hydroxide (NaOH) was acquired from Riedel-deHaën, Germany, while aluminum nitrate nonahydrate ($Al(NO_3)_3.9H_2O$) was obtained from HIMEDIA. Methylene blue hydrate dye was purchased from Fluka. All chemicals were used as received from the vendors, and deionized water was used throughout the study.

2.2. Preparation of Kiwifruit Peel Aqueous Extract. Kiwifruits (10 pieces) were peeled, and the peels were dried in the dark at room temperature and then cut into small pieces. The kiwifruit peels (10 g) were added into 100 mL of deionized water and stirred at room temperature for 18 hr. The extract was then filtered by vacuum, and the resultant filtrate was centrifuged at 6,000 rpm at room temperature. The supernatant was collected and filtered through a syringe filter (0.22 μm). The filtrate was refrigerated for subsequent use [25].

2.3. Total Phenolic Content (TPC). TPC in the kiwifruit peel aqueous extract was determined using the Folin–Ciocalteu reagent as reported by Martínez-Cabanas et al. [26] with some modifications. One hundred microlitres of the extract was diluted with 5 mL of deionized water and mixed with 500 μL of Folin–Ciocalteu reagent. The mixture was shaken vigorously using a vortex mixed for 5 min. In total, 2.5 mL of 5% Na_2CO_3 solution was then added, and the total volume was adjusted to 12 mL with deionized water. The solution mixture was incubated for 60 min at room temperature, after which the absorbance was measured at 750 nm. A gallic acid standard curve was constructed ($y = 1.06x + 0.068$; $R^2 = 0.9966$) to calculate TPC which was expressed in mg gallic acid equivalent per g of extract (mg GAE/g).

2.4. Total Flavonoid Content (TFC). TFC was determined by aluminum nitrate chromogenic method following the method of Yu and coinvestigators with some modifications [27]. One milliliter of the sample was diluted by adding 4.2 mL of 70% ethanol solution, and then reacted with 400 μL of 5% $NaNO_2$ solution. The solution was shaken and allowed to stand for 6 min. Four hundred microlitres of 10% $Al(NO_3)_3$ solution were then added to the solution mixture which was stored for another 6 min. Four milliliters of 4% NaOH solution were next added, and the mixture was incubated for 15 min at room temperature. Absorbance was measured at 410 nm. Rutin standard curve was plotted ($y = 1.0681x + 0.087$; $R^2 = 0.9996$) and used to determine TFC which was expressed in mg rutin equivalent per g of extract (mg RE/g).

2.5. Synthesis of AgNPs Using Kiwifruit Peel Aqueous Extract. A stock solution of silver nitrate ($AgNO_3$) (10 mM, 100 mL) was used to prepare serial dilutions of $AgNO_3$ (5, 2.5, and 1.25 mM). The optimal reaction conditions for the synthesis of AgNPs were obtained by mixing different ratios (v/v) of $AgNO_3$ and kiwifruit peel extract at different temperatures for different reaction times. The formation of the nanoparticles was established visually by

observing the change in color of the reaction mixture from colorless to dark brown as the reaction progressed. AgNPs production was further confirmed by monitoring the absorbance between 450 and 490 nm on a UV–vis spectrometer. The synthesized AgNPs were collected by centrifugation at 6,000 rpm for 15 min. AgNPs were washed thrice using deionized water to remove unreacted salts and extracts. The collected nanoparticles were resuspended in 10 mL of deionized water and stored at 4°C for further use. The concentration of the nanoparticle solution was determined by drying a known volume of the nanoparticles solution in an oven set 120°C.

2.6. Effect of $AgNO_3$ Concentration on AgNPs Synthesis. Kiwifruit peel extract (4 mL) was added to $AgNO_3$ aqueous solution (4 mL) of different concentrations (10, 5, 2.5, and 1.25 mM). The reactants were reacted at room temperature for 2 hr under constant stirring. The formation of AgNPs was monitored visually and by UV–vis spectroscopy where the characteristic absorption band appeared at λ_{max} 480 nm [28].

2.7. Effect of Kiwifruit Peel Extract Amount on AgNPs Synthesis. The effect of the concentration of kiwifruit peel extract on AgNPs synthesis was studied at room temperature by mixing different ratios of extract with respect to $AgNO_3$ (1 : 1, 1 : 2, 1 : 3, 1 : 4, 3 : 1, 7 : 1 $AgNO_3$:extract *v*/*v*). The reaction mixture was allowed to stir for 2 hr, after which a brown color developed. The formation of the AgNPs was monitored by UV–vis spectroscopy. The ratio that yielded the highest intensity absorption band at λ_{max} 480 nm was chosen for further optimization. The most intense surface plasmon resonance (SPR) band was recorded for 1 : 3 $AgNO_3$:extract [28].

2.8. Effect of Temperature. The effect of temperature on the assembly of AgNPs was investigated at three different temperatures, namely 25, 50, and 80°C at 1 : 3 $AgNO_3$ (10 mM): extract ratio (2 mL $AgNO_3$ + 6 mL kiwifruit extract). The mixtures were stirred magnetically for 2 hr, after which the UV–vis spectrum of the mixture was collected and the absorption band at λ_{max} 480 nm was monitored.

2.9. Effect of Reaction Time. The effect of reaction time on AgNPs formation was studied at room temperature by mixing 1 : 3 $AgNO_3$ (10 mM):extract ratio (2 mL $AgNO_3$ + 6 mL kiwifruit peel extract). Aliquots were taken at different time intervals (0–5 hr), and the formation of the AgNPs was monitored by UV–vis spectroscopy. The intensity of the absorption peak increased progressively with time due to the continuous formation of AgNPs [29].

2.10. Characterization of Synthesized AgNPs. TGA was performed on a Bruker TGA-IR Tensor 27 NETZSCH TG 209 F1 LIBRA under N_2 atmosphere. Samples (12 mg) were placed in a 100 μL Al_2O_3 crucible and heated from 30 to 1,100°C with a heating rate of 10°C/min. X-ray diffraction (XRD) diffractograms were collected on D8 FOCUS XRD (BRUKER) employing Cu-k_α radiation ($k_\alpha = 0.154$ nm) in the range $5° \leq 2\theta \leq 80°$, where 100 mg of sample were placed in the sample holder. Transmission electron microscopy (TEM) micrographs were obtained on a JEOL 1400 plus transmission electron microscope operated at 80 kV, by placing ~2 mg of dried sample on a copper grid. The morphology of the prepared nanoparticles was examined on a MIRA 3 TESCAN Czechia scanning electron microscope operating with a beam voltage of 15–30 kV. The nanoparticles (~2 mg) were placed on aluminum stubs using conductive double-coated carbon tape and sputter-coated with a thin layer of platinum using Quorum 150 V Plus (UK) sputter coater. The elemental composition of AgNPs was assessed by energy dispersive X-ray (EDX) spectroscopy equipped with detector-type SDD Apollo X at an accelerating voltage of 20 kV. The average hydrodynamic diameter, polydispersity index, and zeta (ζ) potential of nanoparticles were determined by dynamic light scattering (DLS) in water at 25°C using NanoPlus HD® DLS, USA. The characteristic functional groups of AgNPs and plant extract were elucidated by collecting fourier transform infrared (FTIR) spectra on an FTIR NICOLET iS5 in the range 400–4,000 cm^{-1}, where ~1 mg of sample was mixed with 100 mg of anhydrous potassium bromide (KBr) and pressed into a pellet. UV–vis spectra were collected using a JASCO V−670 spectrophotometer in the range of 350–700 nm.

2.11. Degradation of Methylene Blue Dye. A stock solution of methylene blue (0.01 mg/mL) was prepared by dissolving 5 mg of the dye in 500 mL of deionized water. The experiment was conducted by mixing 2 mL of freshly prepared aqueous $NaBH_4$ solution (0.2 M), 50 mL of the methylene blue stock solution, and 50 μL of AgNPs (8 mg/mL). A mixture with no nanoparticles added was used as a negative control. Catalytic degradation of the dye was assessed by withdrawing 4 mL aliquots at different time intervals and monitoring the dye's characteristic absorption band at 660 nm using UV-visible spectrophotometer. The catalytic efficiency was measured according to the following equation:

$$\text{Catalytic efficiency (CE(\%))} = (A_o - A_t)/A_o \times 100, \quad (1)$$

where A_o is the initial absorbance of the dye solution (before AgNPs addition), and A_t is the absorbance of the dye solution after time t in the presence of nanoparticles.

3. Results and Discussion

3.1. Visual Indication of the Successful Green Synthesis of AgNPs. The current study started by testing the utility of the aqueous kiwifruit peel extract as a potential reducing agent for the bioreduction of the Ag^+ ions into AgNPs. To achieve this goal, 1 : 1 ratio (*v*/*v*) of $AgNO_3$ (10 mM) and kiwifruit peel aqueous extract were stirred at room temperature for 2 hr. The color of the mixture changed as the reaction progressed from pale yellow to dark brown, thus providing visual evidence for the successful formation of AgNPs (Figure 1). The formation of AgNPs was further validated by collecting UV–vis spectra where the characteristic SPR band appeared in the range of 450–490 nm (Figure 1). The unique optical properties of AgNPs permit its interaction with particular light wavelengths. Free electrons on the surface of the nanoparticles get excited and hence oscillate collectively giving rise to the SPR absorption

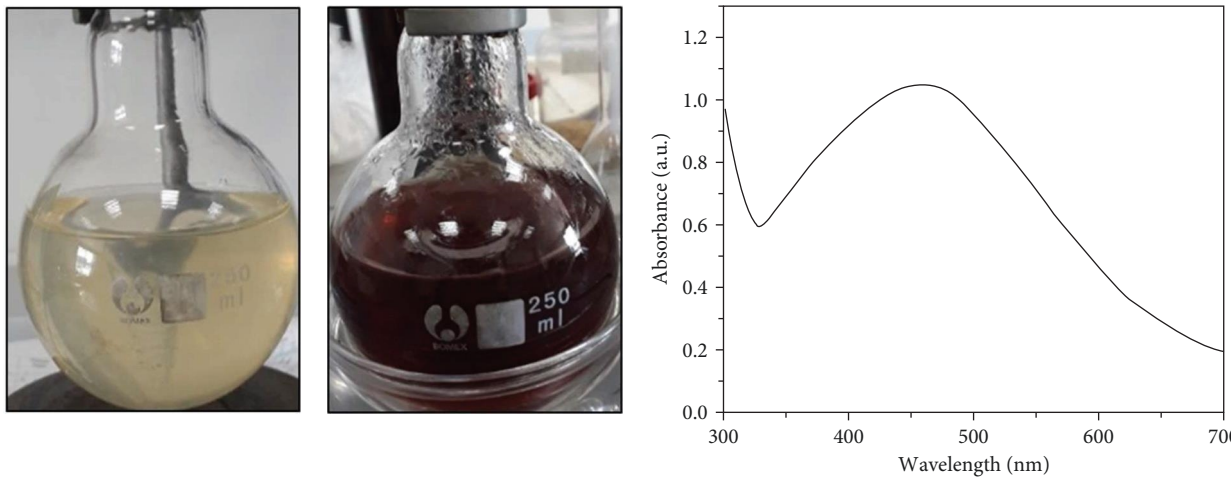

Figure 1: Mixture of kiwifruit peel extract and $AgNO_3$ at $t = 0$ min (a) and $t = 2$ hr (b). Change of color of the reaction mixture from pale yellow to brown indicated the formation of AgNPs. (c) UV–vis spectrum of biosynthesized AgNPs with SPR band appearing at 480 nm.

band. It is important to note that the characteristic UV–vis absorption band of AgNPs can exhibit significant blue or red shifts depending on various factors, including the size and shape of the particles, agglomeration, and dielectric perturbations of the surrounding medium [30, 31]. In fact, a shift to higher wavelengths accompanied by band broadening suggests an increase in particle size. On the other hand, smaller particles are usually associated with sharper absorption bands occurring at shorter wavelengths. Furthermore, it has been reported that a change in the plant extract concentration can significantly affect the size and size distribution of the biosynthesized AgNPs [32].

3.2. Total Phenolic and Total Flavonoid Contents. It has been reported in numerous sources that the successful green synthesis of AgNPs using plant extracts was attributed to the presence of bioreducing phytochemicals such as phenolic compounds, flavonoids, and polysaccharides [33, 34]. Therefore, we set out to determine the total phenolic and total flavonoid content in the kiwifruit peel aqueous extract. Interestingly, the kiwifruit peel aqueous extract was rich in phenolic compounds and flavonoids with TPC and TFC levels of 16.66 ± 0.64 mg GAE/g and 20.25 ± 3.11 mg RE/g, respectively. These values are higher compared to those reported by Alim et al. [35] where the total phenolic and flavonoid contents were 12.8 mg GAE/g DW and 2.7 mg RE/g DW, respectively, in kiwifruit peel extract. The novelty of using the kiwifruit peel extract stems not only from utilizing an otherwise rejected side product but also from the fact that peels are richer in total phenolic and flavonoid contents compared to the flesh as corroborated in multiple reports [35–37]. Such high levels of phenolic compounds and flavonoids in the extract utilized in the current study render them ideal for nanoparticles synthesis.

3.3. Optimization of the Green Synthesis of AgNPs. The optimal reaction conditions for the green preparation of AgNPs were attained by varying different reaction parameters such as ratios of the reactants, reaction temperature, and time. The progress of the reactions and the assembly of AgNPs was monitored by tracking the SPR band at 480 nm with the UV–vis spectrometer.

3.3.1. Effect of $AgNO_3$ Concentration on Kiwifruit Peel Extract-Mediated AgNPs Synthesis. The optimal $AgNO_3$ concentration for the preparation of AgNPs was assessed by mixing a fixed volume of the kiwifruit peel extract with increasing concentrations of $AgNO_3$ (1.25 mM−10 mM) (1 : 1 v/v) at room temperature for 2 hr. The formation of the nanoparticles was examined visually through the development of a dark brown color and confirmed spectrometrically on a UV–vis spectrometer. It was obvious that the formation of the nanoparticles was promoted by increasing $AgNO_3$ concentration as reflected in the enhancement of the SPR band intensity at 480 nm, with the highest absorption observed at 10 mM $AgNO_3$ (Figure 2). It is possible that when the concentrations of $AgNO_3$ increased, greater amounts of accessible Ag^+ ions were converted to AgNPs by the reducing agents found in the plant extract. These results are in agreement with previous studies which described similar observations [38–40]. Therefore, $AgNO_3$ concentration of 10 mM was chosen for further optimization studies. It should be noted that a red shift was observed for SPR band at higher $AgNO_3$ concentrations. This shift can be attributed to the agglomeration of smaller particles to bigger ones according to Mie's theory [41, 42].

3.3.2. Effect of $AgNO_3$: Extract Ratio on the Formation of AgNPs. The optimal ratio of $AgNO_3$:kiwifruit peel extract that will yield the highest amount of nanoparticles was determined by reacting different ratios of the reactants (1 : 1, 1 : 2, 1 : 3, 1 : 4, 3 : 1, 7 : 1 $AgNO_3$:extract *v*/*v*). The reaction mixture was stirred for 24 hr at room temperature, and the generation of the AgNPs was tracked by monitoring the SPR band at 480 nm by UV–vis spectrometry, as depicted in Figure 3. Interestingly, lower amounts of nanoparticles were afforded

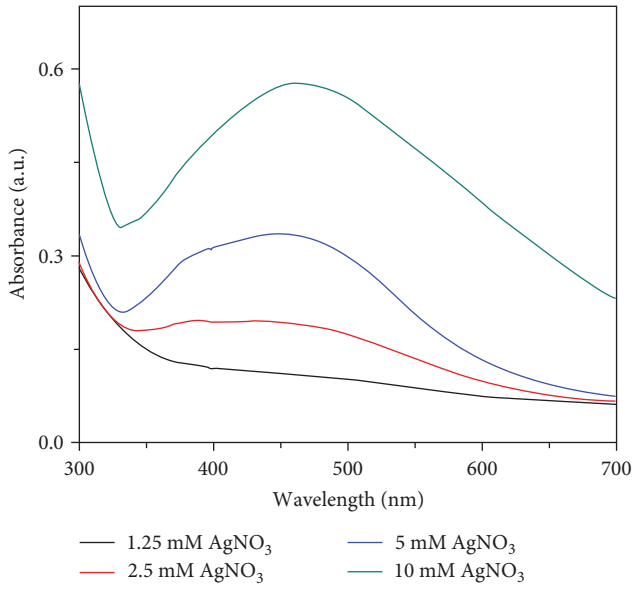

(a)

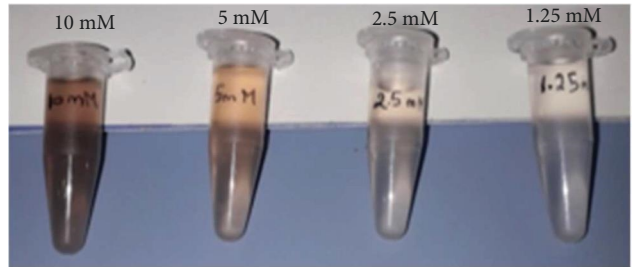

(b)

Figure 2: (a) UV–vis spectra of AgNPs prepared by mixing a fixed concentration of the extract and varying concentrations of $AgNO_3$. The reaction was performed at room temperature for 2 hr. The peak at 480 nm is indexed to the SPR band of AgNPs. (b) Color change in the reaction mixture at different concentrations of $AgNO_3$, where darker color indicated higher amounts of nanoparticle formation.

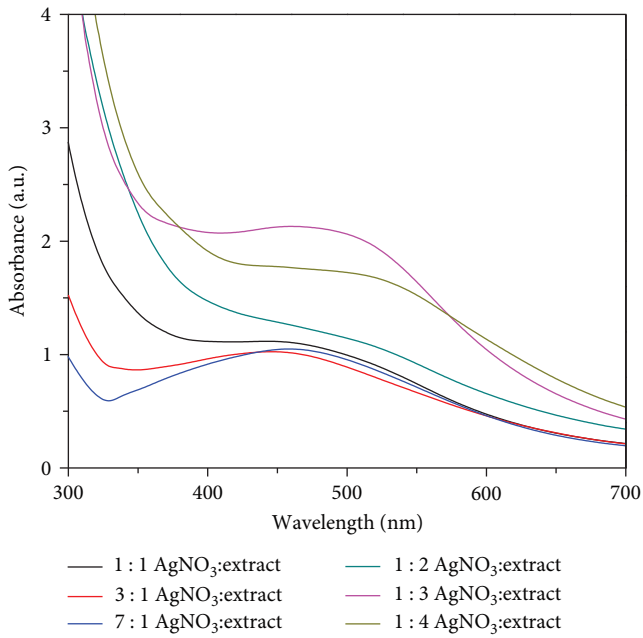

Figure 3: UV–vis spectra of AgNPs prepared at varying ratios of $AgNO_3$ and kiwifruit peel extract. Reactions were performed at room temperature for 24 hr.

when higher amounts of silver ions with respect to the plant extract (i.e., 3 : 1 and 7 : 1 $AgNO_3$:extract) were used. This can be attributed to the fact that large amounts of silver ions combined with a little amount of reducing agent from the kiwifruit peel extract will result in the generation of less AgNPs. Consequently, fewer conduction electrons are oscillating on the surface of nanoparticles upon activation by a wavelength of light, resulting in a decrease in intensity of the SPR band. On the other hand, deploying larger amounts of the plant extract (i.e., 1 : 1, 1 : 2, 1 : 3, and 1 : 4 $AgNO_3$:extract) stimulated reduction of more Ag^+ ions into Ag^o nanoparticles as reflected in the increased intensity of the SPR band in the UV–vis spectrum. The largest amount of nanoparticles was attained at 1 : 3 $AgNO_3$:extract *v*/*v*. This is consistent with the work of Masum et al. [43] who reported that the SPR spectra of AgNPs prepared at high concentrations of *Phyllanthus emblica* fruit extract exhibited sharper and stronger SPR absorption bands. Such phenomenon was attributed to the increasing rate of spontaneous nucleation at higher plant extract concentration containing larger amounts of bioreductants which significantly accelerated the growth rate of AgNPs [44].

3.3.3. Effect of Temperature on Nanoparticles Synthesis. Temperature is a crucial parameter that can influence the synthesis of AgNPs in terms of yield and particle size. In the current study, the effect of temperature on AgNPs synthesis was studied at room temperature (25), 50, and 80°C where the reactants were mixed at 1 : 3 ratio of $AgNO_3$:extract (*v*/*v*). The corresponding UV–vis spectra depicted in Figure 4 showed that an increase in the reaction temperature caused a significant increase in the intensity of the SPR band, with the highest intensity observed at 80°C. These results suggested that at higher temperatures, the rate of the reaction increases causing the reduction of more Ag^+ ions into AgNPs. Moreover, the increase in reaction temperature was associated with a blue shift in the SPR band indicating the formation of smaller AgNPs. The rapid reduction of silver ions at higher temperatures culminated in the homogenous nucleation of silver nuclei leading to the formation of smaller AgNPs. Conversely,

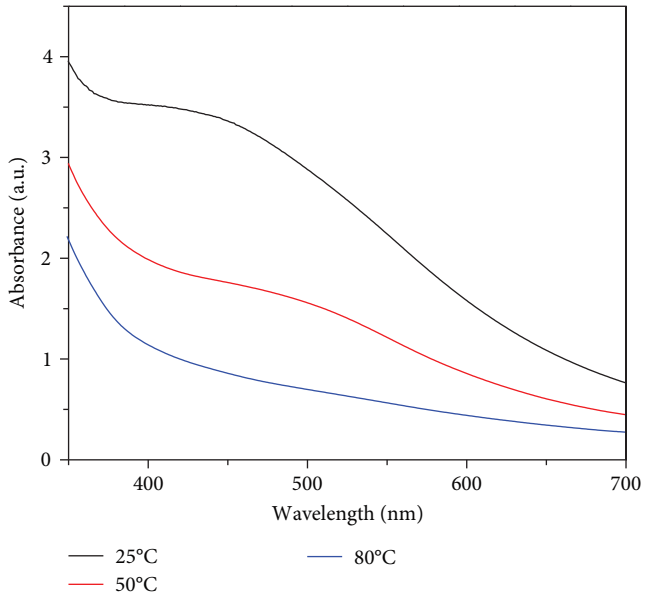

Figure 4: Effect of temperature on the green synthesis of AgNPs from the reaction of $AgNO_3$ and kiwifruit peel extract at 1 : 3 ratio, respectively.

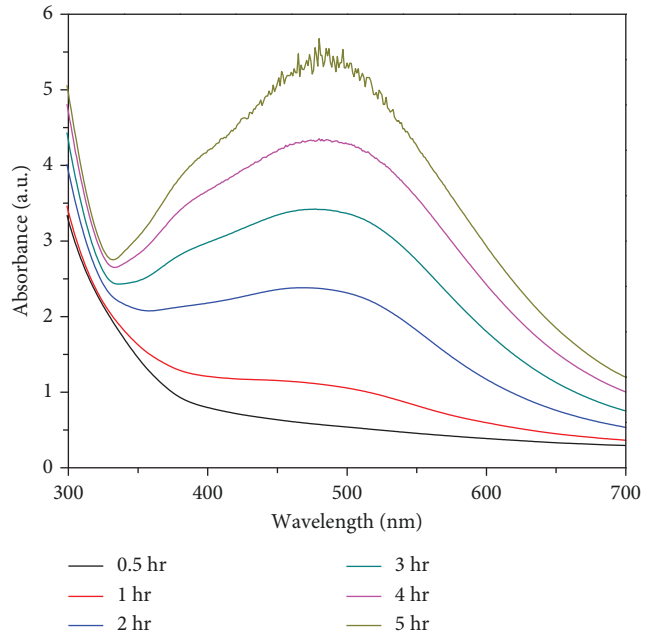

Figure 5: UV–vis spectra highlighted the effect of reaction time on the absorbance intensity of green synthesized AgNPs prepared at room temperature.

lower temperatures caused band broadening and reflected the formation of large-sized AgNPs [29].

3.3.4. Effect of Reaction Time on AgNPs Synthesis. UV–vis spectra of the green synthesized AgNPs prepared at room temperature by mixing 1 : 3 $AgNO_3$:extract (*v*/*v*) were collected at different time intervals, as depicted in Figure 5. Monitoring the kinetics of the reaction by UV–vis spectroscopy showed that the formation of the nanoparticles was time dependent. The characteristic SPR band at 480 nm did not appear after 0.5 hr indicating that no AgNPs were formed. However, nucleation occurred after 1 hr, and the generation of AgNPs was tracked by observing the steady increase in the intensity of the absorption band as the reaction progressed for 5 hr. The optimal reaction time for the preparation of biologically synthesized AgNPs is influenced by several parameters including reactant concentrations, reaction temperature, and the nature of the green reducing agent used in the synthesis. Therefore, the time needed for complete reduction of the Ag^+ ions varied in different literature reports from 1 to 124 hr [29, 38, 45–48].

3.3.5. Optimal Conditions for the Green Synthesis of AgNPs. The culmination of the optimization experiments described before led to the development of optimal reaction conditions for the preparation of silver nanoparticles using kiwifruit peel extract as a bioreducing agent. The proposed experimental setup involved reacting 1 : 3 ratio of $AgNO_3$:extract (*v*/*v*) at room temperature for 2 hr to allow maximal nucleation of AgNPs as suggested by the change in the reaction color from pale yellow to brown. The reaction mixture is then heated at 80°C for an additional 2 hr to allow the growth of the Ag^0 nuclei into nanoparticles associated with the development of a dark brown color. Figure 6 depicts a schematic illustration for the formation of silver nanoparticles mediated by phytochemicals present in the kiwifruit peel extract. It has been reported that kiwifruit peels are rich in phenolic compounds such as quercetin, rutin, ferulic acid, catechin, caffeic acid, and sinapic acid [23, 35]. These phytochemicals play an essential role in the initiation of nanoparticle formation and its stabilization. With its high redox potential compared to other functional groups, the phenolic hydroxyl groups are the major donors of electrons that transfer to the metal ions causing its reduction. The synthetic scheme consists primarily of three steps. First, the silver ions are complexed into phenoxide groups in phenolic compounds keeping them in close proximity to the electron source. This step is followed by nucleation where Ag^+ ions accept electrons from the phytochemicals and are reduced to Ag^0 thus forming the seeds for the growth and maturation of silver nanoparticles. Consequently, the phenolic hydroxyl groups are oxidized to the quinone keto form that serves, among others, as a stabilizing agent for the growing nanoparticles [49, 50].

3.4. Characterization of Green AgNPs

3.4.1. Size, Size Distribution, Surface Morphology, and ζ Potential. The size and morphology of the synthesized nanoparticles were elucidated using different analytical techniques. Micrographs collected by TEM revealed that the optimized reaction conditions led to the biopreparation of quasi-spherical monodisperse nanoparticles having an average diameter of 36 nm (Figures 7(a) and 7(b)). The surface morphology of the nanoparticles was further examined by scanning electron microscopy (SEM) that confirmed the quasispherical shape and uniform distribution of the nanoparticles (Figure 7(c)). The high agglomeration portrayed in

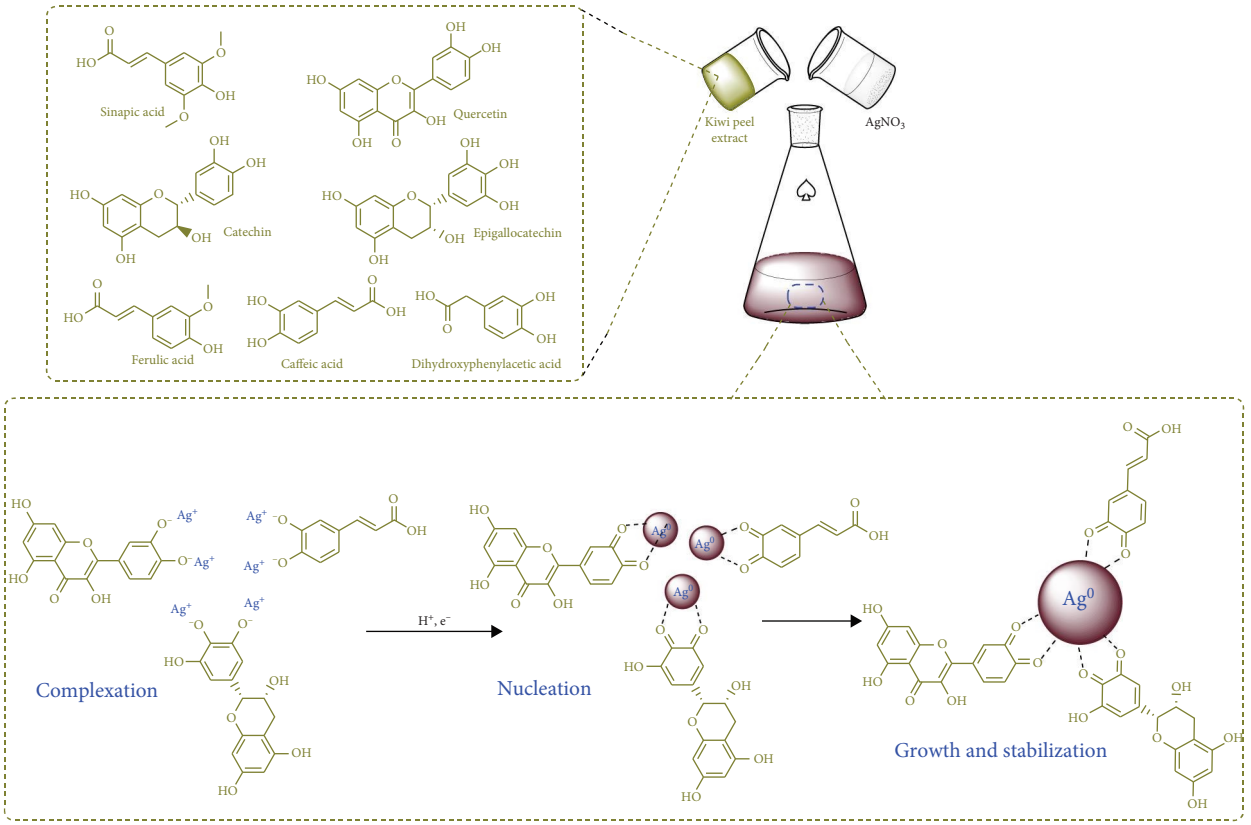

Figure 6: Schematic illustration for the biosynthesis of AgNPs mediated by phytochemicals in kiwifruit peel extract.

the SEM images was possibly a consequence of the dehydration implied during the preparation of samples for SEM microanalysis [25, 51]. The chemical composition of the nanoparticles was analyzed by EDX spectroscopy. The EDX spectrum showed a strong absorption peak for silver at 3 keV, indicating that silver is a major constituent of the nanoparticles (Figure 7(d)). The presence of carbon and oxygen detected in the spectrum was attributed to the organic layer coating the nanoparticles from the kiwifruit peel extract. Not only had the organic compounds functioned as bioreductants, but as stabilizing and capping agents for the biosynthesized nanoparticles as well [20, 52].

The hydrodynamic diameter, size distribution, PDI, and ζ-potential of the biogenic silver nanoparticles were determined by dynamic light scattering (DLS). The hydrodynamic diameter of the nanoparticles was 106 nm, which is much bigger than the size determined from TEM micrographs (36 nm) (Figure 7(e)). In fact, the hydrodynamic size measures the size of the nanoparticle plus the surrounding liquid halo, while TEM measures the actual size of the inorganic silver core only. The low polydispersity index of 0.213 highlighted the monodispersity of the nanoparticles, thus corroborating the conclusions drawn from TEM images. In addition, the presence of an organic brush on the surface of the nanoparticles can contribute to an increase in the hydrodynamic diameter. The presence of a single peak in the DLS spectrum reflected the uniform distribution of nanoparticles. The ζ-potential measurements provide an overview of the particles surface charge and its stability in aqueous environments. The AgNPs biosynthesized in the current study exhibited ζ-potential of -34 mV (Figure 7(f)) probably due to the presence of negatively charged functional groups on the plant's phytochemicals [53]. Such high negative value signifies the superior colloidal stability of the nanoparticles due to electrostatic repulsion that prevents aggregation and leads to enhanced dispersity [25, 54].

3.4.2. XRD Studies. The crystallinity of the biogenic AgNPs was assessed by XRD studies. The obtained diffractogram showed sharp peaks, thus confirming the crystallinity of the synthesized nanoparticles (Figure 8). In particular, the diffraction peaks at 38.30°, 44.47°, 64.86°, and 77.98° were indexed, respectively, to the (1 1 1), (2 0 0), (2 2 0), and (3 1 1) crystallographic planes of face-centered cubic (*fcc*) structure of AgNPs. During crystal growth, Ag atoms appear to preferentially adsorb on the (1 1 1) Bragg plane as inferred by the most intense peak obtained by reflection from the (1 1 1) plane [55]. The observed diffraction pattern matched the standard diffraction pattern of JCPDS file no. 04-0783, thus confirmed the nature of the prepared AgNPs. In addition to the characteristic peaks of the *fcc* silver, several other sharp peaks appeared in the diffractogram and were attributed to the possible crystallization of the organic reducing coating on the surface of AgNPs [30, 56, 57]. The diffraction pattern of these peaks exquisitely matched the standard diffraction pattern corresponding to carbon oxide, suggesting the presence of organic compounds. Furthermore, the collected diffractogram

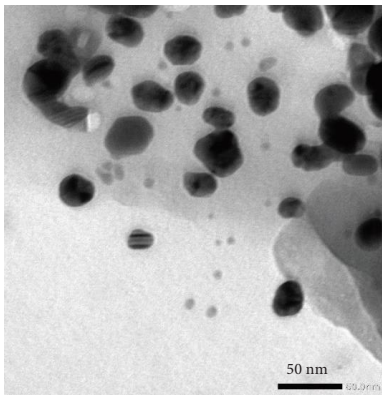

(a)

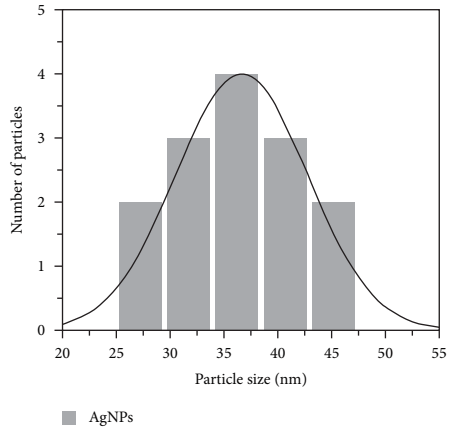

(b)

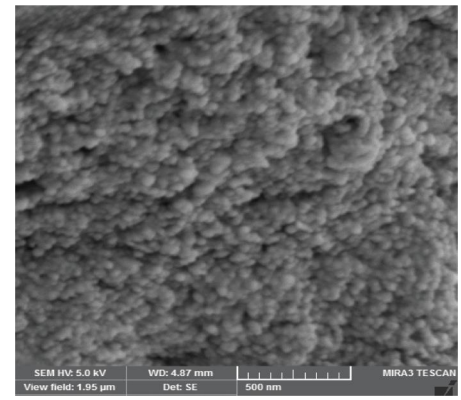

(c)

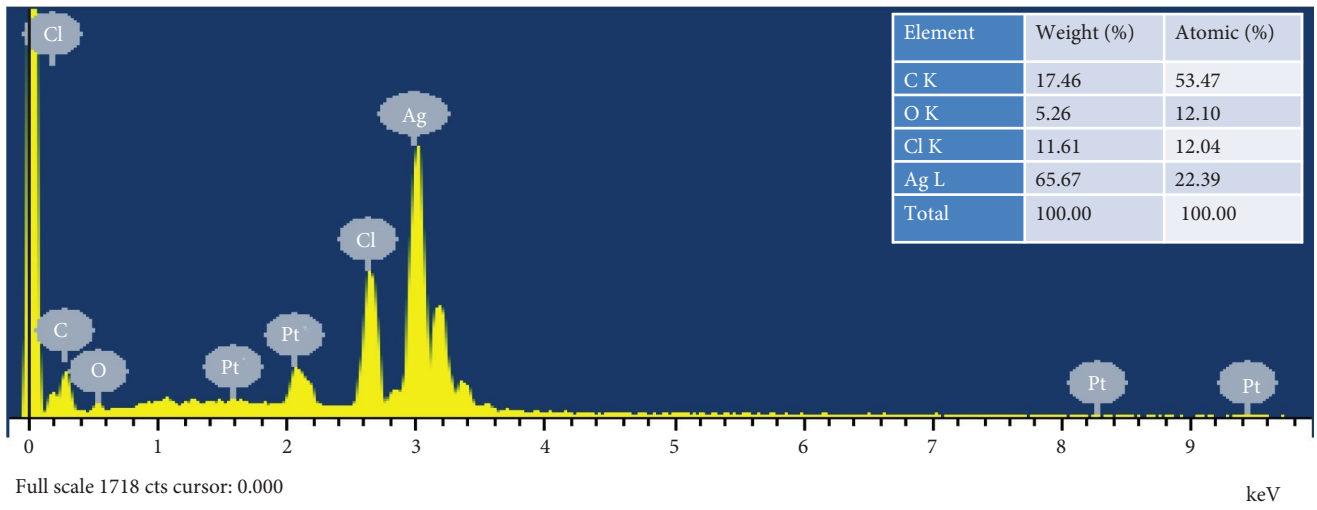

Element	Weight (%)	Atomic (%)
C K	17.46	53.47
O K	5.26	12.10
Cl K	11.61	12.04
Ag L	65.67	22.39
Total	100.00	100.00

(d)

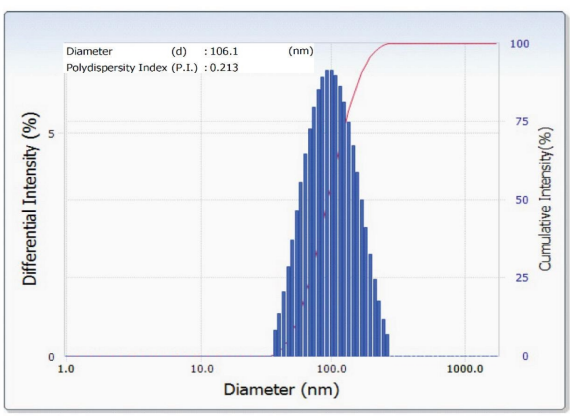

(e)

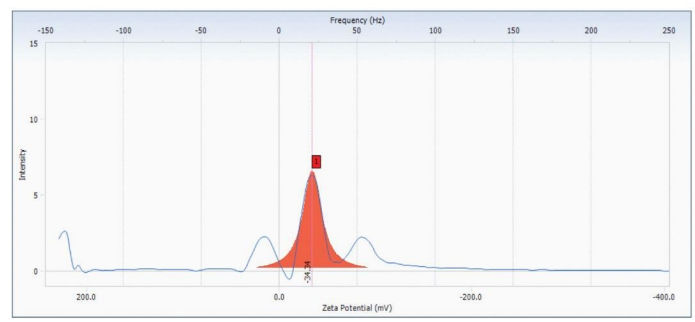

Measurement Results

Zeta Potential	: -34.34	(mV)	Doppler shift	: 21.22	(Hz)
Mobility	: -2.678e-004	(cm²/Vs)	Base Frequency	: 124.0	(Hz)
Conductivity	: 0.0231	(mS/cm)	Conversion Equation	: Smoluchowski	

(f)

FIGURE 7: (a) Transmission electron micrograph of the green synthesized AgNPs. (b) Size distribution histogram of nanoparticles obtained from the TEM image. (c) SEM image and (d) EDX spectrum of the biosynthesized AgNPs. The elemental components and relative abundance are displayed in the inset. (e) Hydrodynamic diameter, size distribution, and polydispersity index of the biosynthesized AgNPs as determined by DLS. (f) ζ-potential of AgNPs.

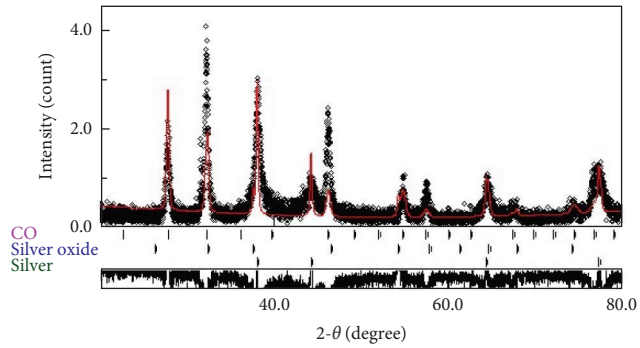

Figure 8: XRD pattern of the synthesized AgNPs.

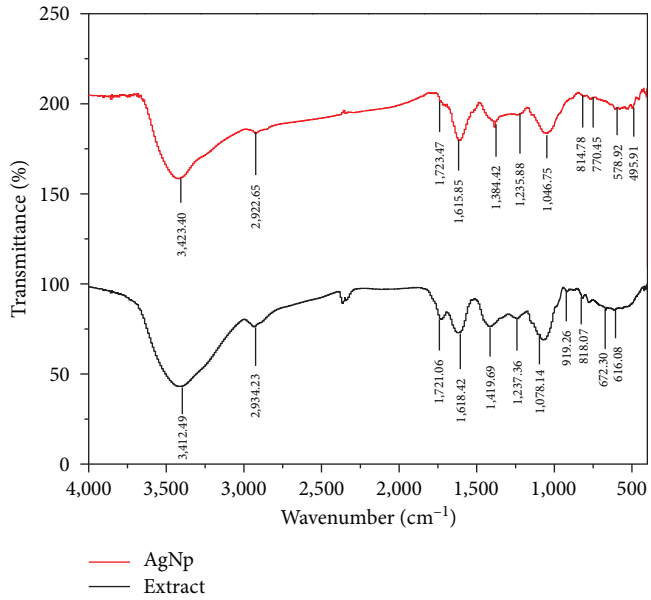

Figure 9: FTIR spectra of the kiwifruit peel extract and the biosynthesized nanoparticles.

revealed that the formation metallic silver (Ag^0) was also accompanied by a minor generation of silver oxide (Ag_2O) (JCPDS file 012-0793).

3.4.3. FTIR Analysis. FTIR spectroscopy was utilized to decipher the functional groups derived from the biomolecules of the kiwifruit peel extract responsible for reducing and capping the biogenic AgNPs. Figure 9 shows the FTIR spectra of the plant extract and that of the biosynthesized nanoparticles [58].

The FTIR absorption spectra of kiwifruit peel extract showed a strong band at 3,412 cm^{-1} attributed to the stretching vibrations of O–H of alcohols and phenols, while the bands at 2,934 and 2,860 cm^{-1} corresponded to the C_{sp3}-H stretching vibrations. The bands recorded at 1,618 and 1,419 cm^{-1} were credited to the C = C stretching vibrations in aromatic systems. The band at 1,721 cm^{-1} corresponds to C = O stretching vibration in esters, carboxylic acids, aldehydes, or ketones. The presence of aliphatic alcohols was further established by the C–O stretching vibration at 1,078 cm^{-1}, while the presence of phenolic hydroxyl groups was supported by the band at 1,237 cm^{-1}. The bands between 700 and 850 cm^{-1} resulted from the out-of-plane (oop) bending vibrations of aromatic = C–H bonds. All of the aforementioned bands were registered in the FTIR spectrum of biogenic AgNPs, suggesting that these groups were responsible for the reduction of Ag^+ ions to Ag^o and enhancing the colloidal stability of the nanoparticles. In fact, the shift in the absorption frequency of some functional groups such as C = O, C–O, and O–H suggested the strong coordination between the respective phytochemicals and the AgNPs. The described functional groups are common in the chemical structure of flavonoids and phenolic acids, which are believed to have acted as reducing agents.

3.4.4. TGA Analysis. The thermal stability of the biosynthesized AgNPs was investigated by TGA, and the corresponding thermograph is depicted in Figure 10. The initial minor weight loss (~4%) occurring below 200°C can be attributed to the moisture associated with the nanoparticles sample. A steady and gradual weight loss started at 200°C and

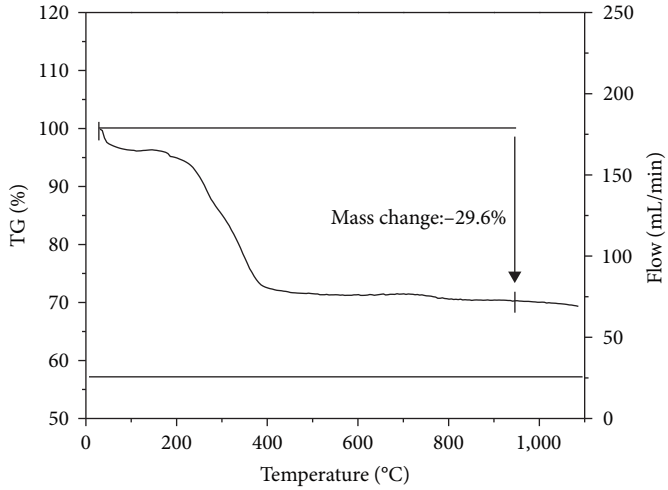

Figure 10: TGA thermograph of the biosynthesized AgNPs.

continued until 400°C after which no major weight loss was observed. This was attributed to the desorption of the bioorganic layer on the nanoparticles which accounted for 30% of the overall nanoparticle weight, which is in agreement with other studies [59, 60]. Therefore, TGA provided further evidence for the presence of an organic coating attached to the surface of the nanoparticles originating from the kiwifruit peel extract.

3.5. AgNPs Catalyzed Degradation of Methylene Blue Dye. The use of the heterocyclic aromatic dye methylene blue in the textile industry has increased in recent years, and its irresponsible discharge into the environment has detrimental effects on human and aquatic life. In addition, the use of dye-polluted water bodies for irrigation can deteriorate the quality of crops and soil. Therefore, treatment prior to its release into nearby water bodies becomes a necessity. Several innovative methods were developed for the degradation of toxic dyes into nonharmful products [61]. These conventional techniques include adsorption, ultrafiltration, chemical, and electrochemical methods. While these methods proved to be effective in the treatment of water, their application is hindered by high costs, inaccessibility to most communities, energy consumption, and the generation of unsafe side products [62]. In this regard, numerous studies reported the use of green synthesized nanoparticles, particularly AgNPs, for the efficient degradation of dyes [63–67]. This approach does not include harmful chemicals usually employed in chemical and biological wastewater treatment practices [68, 69]. Therefore, we set out to illustrate the catalytic activity of the biogenic AgNPs prepared using kiwifruit peel extract as a bioreducing agent for the degradation of methylene blue dye in the presence of $NaBH_4$. Initially, 1.6 mg of the AgNPs were mixed with 50 mL of methylene blue aqueous solution (10 mg/L) and 2 mL of $NaBH_4$ (0.2 M). Interestingly, instant discoloration and degradation of the dye occurred (Figure 11(a)), highlighting the superior efficiency of the prepared AgNPs as a catalyst that can be translated to large-scale applications.

To track the kinetics of the dye degradation process, smaller amounts of nanoparticles were used (0.4 mg), and the degradation of methylene blue was monitored by measuring the dye's characteristic absorption band at 667 nm on a UV–vis spectrophotometer at different time intervals. Figure 11(b) shows the UV–vis spectra for the reduction of methylene blue by the biosynthesized nanoparticles. It is evident that the degradation of the dye started at the onset of nanoparticle addition as revealed by the 30% degradation occurring just after 15 min. As the reaction progressed, a continuous decrease in the intensity of the absorption band at 667 nm was witnessed with ~80% degradation occurring after 3 hr of exposure (Figure 11(c)). The reaction appears to follow second-order kinetics as implied by the linear relationship (Figure 12) obtained by using Equation $(1)/(A_t) = kt + 1/(A_o)$, where k is the rate constant, t is the reaction time, (A_t) is the concentration of the dye at time t, and (A_o) is the concentration of the dye at time $t = 0$. The rate constant for the degradation reaction was 0.01083 $mM^{-1}s^{-1}$. Many of the literature reports indicated that the degradation of methylene blue by biogenic silver nanoparticles fitted pseudo first-order kinetics [62, 70, 71]. In our study, plotting ln A_t/A_o versus time yielded a straight line whose linear relationship was $y = -0.0069x - 0.3598$; $R^2 = 0.9703$. Based on the R^2 values, it was decided the degradation of methylene blue by AgNPs prepared using kiwifruit peel extract followed second-order kinetics ($R^2 = 0.9895$) rather pseudo first order. While it is not valid to directly compare the catalytic efficiency of the green AgNPs prepared in this study with those reported in literature due to the different experimental setups employed in various studies (Table 1), it is evident that the nanoparticles under investigation possessed superior catalytic activity that facilitated the instantaneous reduction of methylene blue at a very low dose (1.6 mg).

3.6. Mechanism of Catalytic Dye Degradation by AgNPs. AgNPs catalyze the degradation of methylene blue dye by acting as an electron relay system that shuttles the electrons from the borohydride anion (donor) to the dye (acceptor). In the absence of AgNPs, the reduction of the dye by $NaBH_4$ is rather thermodynamically favored, but not kinetically due to the large difference in redox potential between them, which

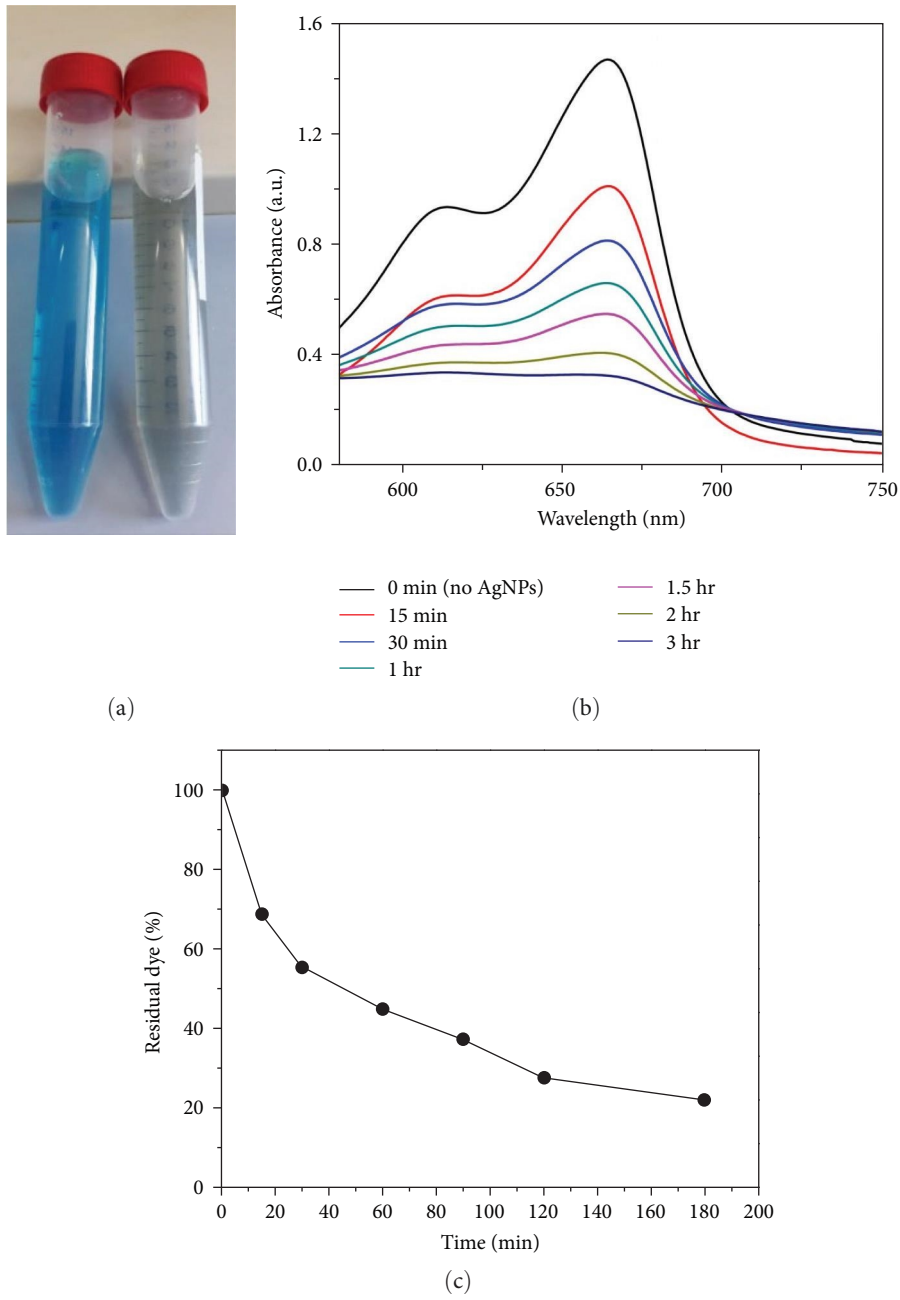

Figure 11: (a) Visual color change from blue to colorless indicating the instantaneous degradation of methylene blue dye. (b) UV–vis absorption spectra for the reduction of methylene blue by $NaBH_4$ catalyzed by 0.4 mg of biosynthesized silver nanoparticles at different time intervals. (c) Catalytic degradation of methylene blue as a function of time.

impedes the transfer of electrons. AgNPs provide an alternative path with lower activation energy, thereby rendering the transfer of electrons between the donor and the acceptor thermodynamically as well as kinetically favorable [55, 81]. Initially, the reactants adsorb onto the surface of AgNPs assisted by the biomolecules capping the nanoparticles. Electrons are first transferred from BH_4^- to AgNPs, which in turn will relay them to the dye, thus inducing its reduction to the Leuco form (Figure 13).

4. Conclusion

The current study provided a detailed, optimized, and eco-friendly approach for the rapid green synthesis of AgNPs using kiwifruit peel aqueous extract as a reducing agent. Optimization of the reaction parameters (i.e., reagents ratio, temperature, and time) emphasized the importance of developing the suitable experimental conditions for high-yielding synthesis of nanoparticles while abiding to the principles of

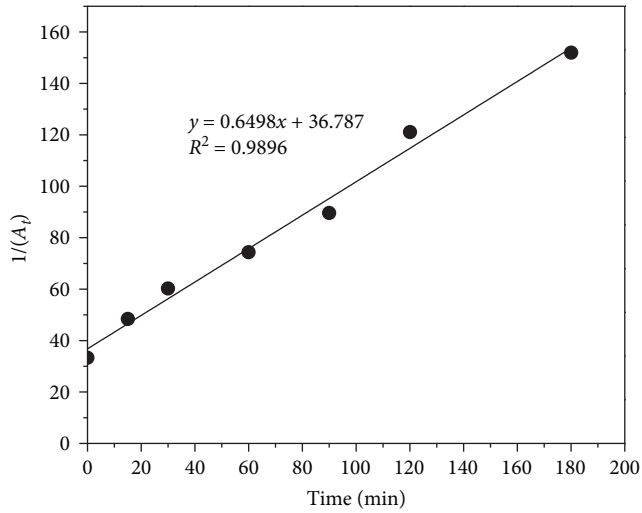

Figure 12: Plot of $1/(A_t)$ against time for the reduction of methylene blue using green synthesized AgNPs. Conditions: (MB) = 0.03 mM, ($NaBH_4$) = 7.7 mM.

Table 1: Comparative analysis of the catalytic efficiency of biosynthesized AgNPs in the degradation of methylene blue (MB).

Plant	Amount of AgNPs	Dye + $NaBH_4$	Incubation time	Degradation (%)	References
Achillea millefolium L.	10 mg	MB (10 ppm, 25 mL) + $NaBH_4$ (250 mM, 25 mL)	13 min	>95%	[72]
Fruit extract of *Gmelina arborea*	3 mL of colloidal AgNPs	MB (10 mM, 10 mL) + $NaBH_4$ (1 mM, 3 mL)	10 min	100%	[66]
Mentha aquatica leaf extract	2.6 μg	MB (0.05 mM) + $NaBH_4$ (0.0083 M); final volume 3 mL	26 min	100%	[73]
Trigonella foenum-graecum L. leaf extract	0.5 mL of AgNPs	MB (0.04 mM, 10 mL) + $NaBH_4$ (0.05 M, 0.5 mL)	20 min	>95%	[74]
Caralluma acutangula leaves	20 μL of AgNPs	0.980 ml of 5 mM $NaBH_4$ + 1 mM MB (0.1 mL)	32 min	>95%	[75]
Imperata cylindrica	1 mL of AgNPs	MB (10 mg/L^{-1}, 50 mL) + $NaBH_4$ (0.2 M, 2 mL)	14 min	92%	[76]
Piper chaba stem extract	Colloidal suspension of AgNPs (53.9 mg/L, 100 μL)	MB (2 ppm, 2 mL) + $NaBH_4$ (600 ppm, 1.5 mL)	8 min	>95%	[77]
Kyllinga brevifolia extract	100 μL AgNPs	MB (30 ppm, 3 mL) + $NaBH_4$ (0.1 M, 1 mL)	1.5 min	>95%	[78]
Leaf extract of *Blumea lacera*	20 mg Ag	MB (80 M) + $NaBH_4$	24 min	56%	[70]
Peltophorum pterocarpum (DC.) leaves	71 nmol of Ag	MB dye (0.1 mM, 2 mL) + $NaBH_4$ (10^{-2} M, 1 mL)	6 min	82%	[79]
Diplazium esculentum extract	3 mg	MB (10 ppm, 10 mL) + $NaBH_4$ (5 mM, 3 mL)	90 min	91%	[80]
Actinidia deliciosa peel extract	1.6 mg	MB (0.03 mM, 50 mL) + $NaBH_4$ (0.2 M, 2 mL)	Instant	>95%	This study

green chemistry. The biogenic AgNPs prepared under the optimized reaction conditions were monodisperse and colloidally stable as inferred from the highly negative ζ potential. The superior monodispersity and colloidal stability of the nanoparticles open numerous research avenues in the biomedical and environmental applications. The metallic silver core exhibited a size of 36 nm, was crystalline with *fcc* structure, and covered by a thick layer of organic material as suggested by XRD analysis and TGA. The utility of AgNPs in environmental applications was examined by testing its catalytic efficiency in the degradation of the hazardous methylene blue dye. AgNPs exhibited outstanding catalytic activity in the degradation of methylene blue where instant discoloration was attained with only 1.6 mg of nanoparticles used.

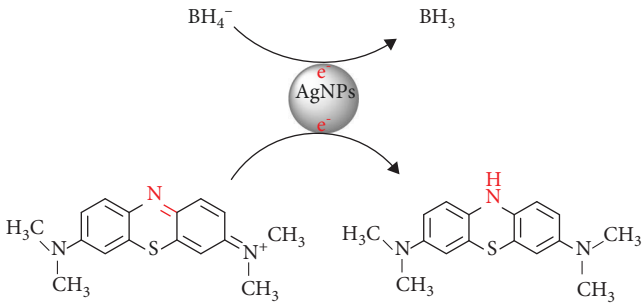

FIGURE 13: Proposed mechanism for the discoloration of methylene blue by sodium borohydride catalyzed by the biosynthesized AgNPs.

Such exceptional activity highlighted the enormous potential of these nanoparticles for integration in water purification systems and dye effluent treatment plants.

Data Availability

The data used to support the findings of this study are included within the article.

Disclosure

The work presented in this paper is published as a preprint [82].

Conflicts of Interest

The authors declare that they have no conflicts of interest.

Acknowledgments

We would like to thank Kamal A. Shair Central Research Science Laboratory, Faculty of Arts and Sciences at the American University of Beirut, for allowing us to use its equipment and facilities to conduct SEM, XRD, TGA, DLS, and ζ potential measurements.

References

[1] M. Azharuddin, G. H. Zhu, D. Das et al., "A repertoire of biomedical applications of noble metal nanoparticles," *Chemical Communications*, vol. 55, no. 49, pp. 6964–6996, 2019.

[2] W. Mei and Q. Wu, "Applications of metal nanoparticles in medicine/metal nanoparticles as anticancer agents," *Metal Nanoparticles*, pp. 169–190, 2018.

[3] A. J. Shnoudeh, I. Hamad, R. W. Abdo et al., "Synthesis, characterization, and applications of metal nanoparticles," in *Biomaterials and Bionanotechnology*, pp. 527–612, Academic Press, 2019.

[4] A. Sápi, T. Rajkumar, J. Kiss, Á. Kukovecz, Z. Kónya, and G. A. Somorjai, "Metallic nanoparticles in heterogeneous catalysis," *Catalysis Letters*, vol. 151, no. 8, pp. 2153–2175, 2021.

[5] S. V. Ganachari, L. Hublikar, J. S. Yaradoddi, and S. S. Math, "Metal oxide nanomaterials for environmental applications," in *Handbook of Ecomaterials*, L. M. T. Martínez, O. V. Kharissova, and B. I. Kharisov, Eds., pp. 2357–2368, Springer International Publishing, Cham, 2019.

[6] S. Vallinayagam, K. Rajendran, and V. Sekar, "Green synthesis and characterization of silver nanoparticles using *Naringi crenulate* leaf extract: key challenges for anticancer activities," *Journal of Molecular Structure*, vol. 1243, Article ID 130829, 2021.

[7] Meenu, M. Rani, and U. Shanker, "Efficient photocatalytic degradation of bisphenol A by green synthesized CuO decorated nickel hexacyanoferrate nanocomposite," *Water and Environment Journal*, vol. 37, no. 3, pp. 428–444, 2023.

[8] S. H. Gebre, "Bio-inspired synthesis of metal and metal oxide nanoparticles: the key role of phytochemicals," *Journal of Cluster Science*, vol. 34, no. 2, pp. 665–704, 2023.

[9] J. Venkatesan, P. K. Gupta, S. E. Son, W. Hur, and G. H. Seong, "Silver-based hybrid nanomaterials: preparations, biological, biomedical, and environmental applications," *Journal of Cluster Science*, vol. 34, no. 1, pp. 23–43, 2023.

[10] M. Z. Alhamid, B. S. Hadi, and A. Khumaeni, "Synthesis of silver nanoparticles using laser ablation method utilizing Nd: YAG laser," *AIP Conference Proceedings*, vol. 2202, no. 1, Article ID 020013, 2019.

[11] R. Vishwanath and B. Negi, "Conventional and green methods of synthesis of silver nanoparticles and their antimicrobial properties," *Current Research in Green and Sustainable Chemistry*, vol. 4, Article ID 100205, 2021.

[12] A. Haider and I.-K. Kang, "Preparation of silver nanoparticles and their industrial and biomedical applications: a comprehensive review," *Advances in Materials Science and Engineering*, vol. 2015, Article ID 165257, 16 pages, 2015.

[13] G. Franceschinis, M. Beverina, M. Corleto et al., "Green-synthesized silver nanoparticles using Aloe maculata extract as antibacterial agent for potential topical application," *OpenNano*, vol. 12, Article ID 100148, 2023.

[14] K. Gudikandula, P. Vadapally, and M. A. S. Charya, "Biogenic synthesis of silver nanoparticles from white rot fungi: their characterization and antibacterial studies," *OpenNano*, vol. 2, pp. 64–78, 2017.

[15] S. Jadoun, R. Arif, N. K. Jangid, and R. K. Meena, "Green synthesis of nanoparticles using plant extracts: a review," *Environmental Chemistry Letters*, vol. 19, no. 1, pp. 355–374, 2021.

[16] D. R. Raj, S. Prasanth, T. V. Vineeshkumar, and C. Sudarsanakumar, "Surface plasmon resonance based fiber optic dopamine sensor using green synthesized silver nanoparticles," *Sensors and Actuators B: Chemical*, vol. 224, pp. 600–606, 2016.

[17] B. Kumar, Y. Angulo, K. Smita, L. Cumbal, and A. Debut, "Capuli cherry-mediated green synthesis of silver nanoparticles under white solar and blue LED light," *Particuology*, vol. 24, pp. 123–128, 2016.

[18] S. F. Hashemi, N. Tasharrofi, and M. M. Saber, "Green synthesis of silver nanoparticles using *Teucrium polium* leaf extract and assessment of their antitumor effects against MNK45 human gastric cancer cell line," *Journal of Molecular Structure*, vol. 1208, pp. 127889–127894, 2020.

[19] K. Logaranjan, A. J. Raiza, S. C. B. Gopinath, Y. Chen, and K. Pandian, "Shape- and size-controlled synthesis of silver nanoparticles using Aloe vera plant extract and their antimicrobial activity," *Nanoscale Research Letters*, vol. 11, no. 1, Article ID 520, 2016.

[20] U. B. Jagtap and V. A. Bapat, "Green synthesis of silver nanoparticles using *Artocarpus heterophyllus* Lam. seed extract and its antibacterial activity," *Industrial Crops and Products*, vol. 46, pp. 132–137, 2013.

[21] H. Alishah, S. P. Seyedi, S. Y. Ebrahimipour, and S. Esmaeili-Mahani, "A green approach for the synthesis of silver

nanoparticles using root extract of *Chelidonium majus*: characterization and antibacterial evaluation," *Journal of Cluster Science*, vol. 27, no. 2, pp. 421–429, 2016.

[22] E. Hsu, "Cost-benefit analysis for recycling of agricultural wastes in Taiwan," *Waste Management*, vol. 120, pp. 424–432, 2021.

[23] F. Cairone, S. Garzoli, L. Menghini et al., "Valorization of Kiwi peels: fractionation, bioactives analyses and hypotheses on complete peels recycle," *Foods*, vol. 11, no. 4, pp. 589–603, 2022.

[24] I. Khan, K. Saeed, I. Zekker et al., "Review on methylene blue: its properties, uses, toxicity and photodegradation," *Water*, vol. 14, no. 2, pp. 242–271, 2022.

[25] Hemlata, P. R. Meena, A. P. Singh, and K. K. Tejavath, "Biosynthesis of silver nanoparticles using *Cucumis prophetarum* aqueous leaf extract and their antibacterial and antiproliferative activity against cancer cell lines," *ACS Omega*, vol. 5, no. 10, pp. 5520–5528, 2020.

[26] M. Martínez-Cabanas, M. López-García, P. Rodríguez-Barro et al., "Antioxidant capacity assessment of plant extracts for green synthesis of nanoparticles," *Nanomaterials*, vol. 11, no. 7, Article ID 1679, 2021.

[27] S. Firoozi, M. Jamzad, and M. Yari, "Biologically synthesized silver nanoparticles by aqueous extract of *Satureja intermedia* C.A. Mey and the evaluation of total phenolic and flavonoid contents and antioxidant activity," *Journal of Nanostructure in Chemistry*, vol. 6, no. 4, pp. 357–364, 2016.

[28] N. Krithiga, A. Rajalakshmi, and A. Jayachitra, "Green synthesis of silver nanoparticles using leaf extracts of *Clitoria ternatea* and *Solanum nigrum* and study of its antibacterial effect against common nosocomial pathogens," *Journal of Nanoscience*, vol. 2015, Article ID 928204, 8 pages, 2015.

[29] S. J. M. Gavade, G. H. Nikam, R. S. Dhabbe, S. R. Sabale, B. V. Tamhankar, and G. N. Mulik, "Green synthesis of silver nanoparticles by using carambola fruit extract and their antibacterial activity," *Advances in Natural Sciences: Nanoscience and Nanotechnology*, vol. 6, no. 4, pp. 045015–045020, 2015.

[30] M. Shaik, M. Khan, M. Kuniyil et al., "Plant-extract-assisted green synthesis of silver nanoparticles using *Origanum vulgare* L. extract and their microbicidal activities," *Sustainability*, vol. 10, no. 4, Article ID 913, 2018.

[31] S. L. Smitha, K. M. Nissamudeen, D. Philip, and K. G. Gopchandran, "Studies on surface plasmon resonance and photoluminescence of silver nanoparticles," *Spectrochimica Acta Part A: Molecular and Biomolecular Spectroscopy*, vol. 71, no. 1, pp. 186–190, 2008.

[32] T. C. Prathna, N. Chandrasekaran, A. M. Raichur, and A. Mukherjee, "Biomimetic synthesis of silver nanoparticles by Citrus limon (lemon) aqueous extract and theoretical prediction of particle size," *Colloids and Surfaces B: Biointerfaces*, vol. 82, no. 1, pp. 152–159, 2011.

[33] M. Pradeep, D. Kruszka, P. Kachlicki, D. Mondal, and G. Franklin, "Uncovering the phytochemical basis and the mechanism of plant extract-mediated eco-friendly synthesis of silver nanoparticles using ultra-performance liquid chromatography coupled with a photodiode array and high-resolution mass spectrometry," *ACS Sustainable Chemistry & Engineering*, vol. 10, no. 1, pp. 562–571, 2022.

[34] N. Swilam and K. A. Nematallah, "Polyphenols profile of pomegranate leaves and their role in green synthesis of silver nanoparticles," *Scientific Reports*, vol. 10, no. 1, Article ID 14851, 2020.

[35] A. Alim, T. Li, T. Nisar et al., "Antioxidant, antimicrobial, and antiproliferative activity-based comparative study of peel and flesh polyphenols from *Actinidia chinensis*," *Food & Nutrition Research*, vol. 63, pp. 1577–1586, 2019.

[36] E. F. El Azab and H. S. Mostafa, "Phytochemical analysis and antioxidant defense of kiwifruit (*Actinidia deliciosa*) against pancreatic cancer and AAPH-induced RBCs hemolysis," *Journal of Food Science and Technology*, vol. 42, pp. e06021–e06030, 2022.

[37] Y. Wang, L. Li, H. Liu et al., "Bioactive compounds and *in vitro* antioxidant activities of peel, flesh and seed powder of kiwi fruit," *International Journal of Food Science & Technology*, vol. 53, no. 9, pp. 2239–2245, 2018.

[38] S. Ahmed, Saifullah, M. Ahmad, B. L. Swami, and S. Ikram, "Green synthesis of silver nanoparticles using *Azadirachta indica* aqueous leaf extract," *Journal of Radiation Research and Applied Sciences*, vol. 9, no. 1, pp. 1–7, 2016.

[39] S. N. Sinha, D. Paul, N. Halder, D. Sengupta, and S. K. Patra, "Green synthesis of silver nanoparticles using fresh water green alga *Pithophora oedogonia* (Mont.) wittrock and evaluation of their antibacterial activity," *Applied Nanoscience*, vol. 5, no. 6, pp. 703–709, 2015.

[40] A. Sasikala, M. L. Rao, N. Savithramma, and T. N. V. K. V. Prasad, "Synthesis of silver nanoparticles from stem bark of *Cochlospermum religiosum* (L.) Alston: an important medicinal plant and evaluation of their antimicrobial efficacy," *Applied Nanoscience*, vol. 5, no. 7, pp. 827–835, 2015.

[41] T. Wriedt, "Mie theory: a review," in *The Mie Theory*, pp. 53–71, Springer, Berlin Heidelberg, 2012.

[42] W. Haiss, N. T. K. Thanh, J. Aveyard, and D. G. Fernig, "Determination of size and concentration of gold nanoparticles from UV−Vis spectra," *Analytical Chemistry*, vol. 79, no. 11, pp. 4215–4221, 2007.

[43] M. M. I. Masum, M. M. Siddiqa, K. A. Ali et al., "Biogenic synthesis of silver nanoparticles using *Phyllanthus emblica* fruit extract and its inhibitory action against the pathogen *Acidovorax oryzae* strain RS-2 of rice bacterial brown stripe," *Frontiers in Microbiology*, vol. 10, pp. 820–837, 2019.

[44] Y. He, F. Wei, Z. Ma et al., "Green synthesis of silver nanoparticles using seed extract of *Alpinia katsumadai*, and their antioxidant, cytotoxicity, and antibacterial activities," *RSC Advances*, vol. 7, no. 63, pp. 39842–39851, 2017.

[45] H. M. M. Ibrahim, "Green synthesis and characterization of silver nanoparticles using banana peel extract and their antimicrobial activity against representative microorganisms," *Journal of Radiation Research and Applied Sciences*, vol. 8, no. 3, pp. 265–275, 2015.

[46] J. M. Ashraf, M. A. Ansari, H. M. Khan, M. A. Alzohairy, and I. Choi, "Green synthesis of silver nanoparticles and characterization of their inhibitory effects on AGEs formation using biophysical techniques," *Scientific Reports*, vol. 6, no. 1, pp. 20414–20423, 2016.

[47] S. El-Hawary, H. EL-Hefnawy, F. A. Mokhtar et al., "Green synthesis of silver nanoparticles using extract of *Jasminum officinal* L. leaves and evaluation of cytotoxic activity towards bladder, 5637 and breast cancer (MCF-7) cell lines," *International Journal of Nanomedicine*, vol. 15, pp. 9771–9781, 2020.

[48] T. R. Santiago, C. C. Bonatto, M. Rossato et al., "Green synthesis of silver nanoparticles using tomato leaf extract and their entrapment in chitosan nanoparticles to control bacterial

wilt," *Journal of the Science of Food and Agriculture*, vol. 99, no. 9, pp. 4248–4259, 2019.

[49] T. N. J. I. Edison, R. Atchudan, and Y. R. Lee, "Optical sensor for dissolved ammonia through the green synthesis of silver nanoparticles by fruit extract of *Terminalia chebula*," *Journal of Cluster Science*, vol. 27, no. 2, pp. 683–690, 2016.

[50] S. M. A. Nayem, N. Sultana, M. A. Haque et al., "Green synthesis of gold and silver nanoparticles by using *Amorphophallus paeoniifolius* tuber extract and evaluation of their antibacterial activity," *Molecules*, vol. 25, no. 20, Article ID 4773, 2020.

[51] M. Sigamoney, S. Shaik, P. Govender, S. B. N. Krishna, and Sershen, "African leafy vegetables as bio-factories for silver nanoparticles: a case study on *Amaranthus dubius* C Mart. Ex Thell," *South African Journal of Botany*, vol. 103, pp. 230–240, 2016.

[52] A. G. Femi-Adepoju, A. O. Dada, K. O. Otun, A. O. Adepoju, and O. P. Fatoba, "Green synthesis of silver nanoparticles using terrestrial fern (*Gleichenia Pectinata* (Willd.) C. Presl.): characterization and antimicrobial studies," *Heliyon*, vol. 5, no. 4, pp. e01543–e01560, 2019.

[53] E.-Y. Ahn, H. Jin, and Y. Park, "Assessing the antioxidant, cytotoxic, apoptotic and wound healing properties of silver nanoparticles green-synthesized by plant extracts," *Materials Science and Engineering: C*, vol. 101, pp. 204–216, 2019.

[54] A. V. A. Mariadoss, V. Ramachandran, V. Shalini et al., "Green synthesis, characterization and antibacterial activity of silver nanoparticles by *Malus domestica* and its cytotoxic effect on (MCF-7) cell line," *Microbial Pathogenesis*, vol. 135, pp. 103609–103616, 2019.

[55] S. Joseph and B. Mathew, "Facile synthesis of silver nanoparticles and their application in dye degradation," *Materials Science and Engineering: B*, vol. 195, pp. 90–97, 2015.

[56] S. Ponarulselvam, C. Panneerselvam, K. Murugan, N. Aarthi, K. Kalimuthu, and S. Thangamani, "Synthesis of silver nanoparticles using leaves of *Catharanthus roseus* Linn. G. Don and their antiplasmodial activities," *Asian Pacific Journal of Tropical Biomedicine*, vol. 2, no. 7, pp. 574–580, 2012.

[57] H. Singh, J. Du, P. Singh, and T. H. Yi, "Ecofriendly synthesis of silver and gold nanoparticles by *Euphrasia officinalis* leaf extract and its biomedical applications," *Artificial Cells, Nanomedicine, and Biotechnology*, vol. 46, no. 6, pp. 1163–1170, 2018.

[58] P. Devaraj, P. Kumari, C. Aarti, and A. Renganathan, "Synthesis and characterization of silver nanoparticles using cannonball leaves and their cytotoxic activity against MCF-7 cell line," *Journal of Nanotechnology*, vol. 2013, Article ID 598328, 5 pages, 2013.

[59] S. Yallappa, J. Manjanna, and B. L. Dhananjaya, "Phytosynthesis of stable Au, Ag and Au-Ag alloy nanoparticles using J. Sambac leaves extract, and their enhanced antimicrobial activity in presence of organic antimicrobials," *Spectrochimica Acta Part A: Molecular and Biomolecular Spectroscopy*, vol. 137, pp. 236–243, 2015.

[60] L. David and B. Moldovan, "Green synthesis of biogenic silver nanoparticles for efficient catalytic removal of harmful organic dyes," *Nanomaterials*, vol. 10, no. 2, pp. 202–217, 2020.

[61] S. Marimuthu, A. J. Antonisamy, S. Malayandi et al., "Silver nanoparticles in dye effluent treatment: a review on synthesis, treatment methods, mechanisms, photocatalytic degradation, toxic effects and mitigation of toxicity," *Journal of Photochemistry and Photobiology B: Biology*, vol. 205, Article ID 111823, 2020.

[62] D. Gola, A. kriti, N. Bhatt et al., "Silver nanoparticles for enhanced dye degradation," *Current Research in Green and Sustainable Chemistry*, vol. 4, pp. 100132–100139, 2021.

[63] K. Sharma, G. Singh, G. Singh, M. Kumar, and V. Bhalla, "Silver nanoparticles: facile synthesis and their catalytic application for the degradation of dyes," *RSC Advances*, vol. 5, no. 33, pp. 25781–25788, 2015.

[64] A. M. Atta, Y. M. Moustafa, H. A. Al-Lohedan, A. O. Ezzat, and A. I. Hashem, "Methylene blue catalytic degradation using silver and magnetite nanoparticles functionalized with a Poly(ionic liquid) based on quaternized dialkylethanolamine with 2-Acrylamido-2-methylpropane Sulfonate-*co*-vinylpyrrolidone," *ACS Omega*, vol. 5, no. 6, pp. 2829–2842, 2020.

[65] J. Kadam, P. Dhawal, S. Barve, and S. Kakodkar, "Green synthesis of silver nanoparticles using cauliflower waste and their multifaceted applications in photocatalytic degradation of methylene blue dye and Hg^{2+} biosensing," *SN Applied Sciences*, vol. 2, no. 4, pp. 738–753, 2020.

[66] J. Saha, A. Begum, A. Mukherjee, and S. Kumar, "A novel green synthesis of silver nanoparticles and their catalytic action in reduction of methylene blue dye," *Sustainable Environment Research*, vol. 27, no. 5, pp. 245–250, 2017.

[67] S. S. Emmanuel and A. A. Adesibikan, "Bio-fabricated green silver nano-architecture for degradation of methylene blue water contaminant: a mini-review," *Water Environment Research*, vol. 93, no. 12, pp. 2873–2882, 2021.

[68] S. Samuchiwal, D. Gola, and A. Malik, "Decolourization of textile effluent using native microbial consortium enriched from textile industry effluent," *Journal of Hazardous Materials*, vol. 402, Article ID 123835, 2021.

[69] S. Pandey, J. Y. Do, J. Kim, and M. Kang, "Fast and highly efficient catalytic degradation of dyes using κ-carrageenan stabilized silver nanoparticles nanocatalyst," *Carbohydrate Polymers*, vol. 230, Article ID 115597, 2020.

[70] P. K. Pandey, J. Sarkar, and S. Srivastava, "Catalytic dye degradation of textile dye methylene blue by using silver nanoparticles fabricated by sustainable approach," *Engineering Proceedings*, vol. 37, no. 1, Article ID 16, 2023.

[71] C. K. Githala, S. Raj, A. Dhaka, S. C. Mali, and R. Trivedi, "Phyto-fabrication of silver nanoparticles and their catalytic dye degradation and antifungal efficacy," *Frontiers in Chemistry*, vol. 10, Article ID 994721, 2022.

[72] B. Khodadadi, M. Bordbar, and M. Nasrollahzadeh, "*Achillea millefolium* L. extract mediated green synthesis of waste peach kernel shell supported silver nanoparticles: application of the nanoparticles for catalytic reduction of a variety of dyes in water," *Journal of Colloid and Interface Science*, vol. 493, pp. 85–93, 2017.

[73] A. Nouri, M. T. Yaraki, A. Lajevardi, Z. Rezaei, M. Ghorbanpour, and M. Tanzifi, "Ultrasonic-assisted green synthesis of silver nanoparticles using *Mentha aquatica* leaf extract for enhanced antibacterial properties and catalytic activity," *Colloid and Interface Science Communications*, vol. 35, Article ID 100252, 2020.

[74] M. Moond, S. Singh, S. Sangwan et al., "Biosynthesis of silver nanoparticles utilizing leaf extract of *Trigonella foenum-graecum* L. for catalytic dyes degradation and colorimetric sensing of Fe^{3+}/Hg^{2+}," *Molecules*, vol. 28, no. 3, Article ID 951, 2023.

[75] W. M. Alamier, N. Hasan, S. K. Ali, and M. D. Y. Oteef, "Biosynthesis of Ag nanoparticles using *Caralluma acutangula* extract and its catalytic functionality towards degradation of

hazardous dye pollutants," *Crystals*, vol. 12, no. 8, Article ID 1069, 2022.

[76] A. A. Fairuzi, N. N. Bonnia, R. M. Akhir, M. A. Abrani, and H. M. Akil, "Degradation of methylene blue using silver nanoparticles synthesized from *Imperata cylindrica* aqueous extract," *IOP Conference Series: Earth and Environmental Science*, vol. 105, no. 1, Article ID 012018, 2018.

[77] M. Mahiuddin, P. Saha, and B. Ochiai, "Green synthesis and catalytic activity of silver nanoparticles based on *Piper chaba* stem extracts," *Nanomaterials*, vol. 10, no. 9, Article ID 1777, 2020.

[78] N. Isa and Z. Lockman, "Methylene blue dye removal on silver nanoparticles reduced by *Kyllinga brevifolia*," *Environmental Science and Pollution Research*, vol. 26, no. 11, pp. 11482–11495, 2019.

[79] S. A. Ogundare, T. O. Adesetan, G. Muungani et al., "Catalytic degradation of methylene blue dye and antibacterial activity of biosynthesized silver nanoparticles using *Peltophorum pterocarpum* (DC.) leaves," *Environmental Science: Advances*, vol. 2, no. 2, pp. 247–256, 2023.

[80] A. A. Hadi, J. Y. Ng, M. Shamsuddin, J. Matmin, and N. A. N. N. Malek, "Green synthesis of silver nanoparticles using *Diplazium esculentum* extract: catalytic reduction of methylene blue and antibacterial activities," *Chemical Papers*, vol. 76, no. 1, pp. 65–77, 2022.

[81] K. Mallick, M. Witcomb, and M. Scurrell, "Silver nanoparticle catalysed redox reaction: an electron relay effect," *Materials Chemistry and Physics*, vol. 97, no. 2-3, pp. 283–287, 2006.

[82] M. K. Agha, B. Maatouk, R. Mhanna, and M. El-Dakdouki, "WITHDRAWN: biosynthesis of silver nanoparticles using *Actinidia deliciosa* peels extract: optimization, characterization, and catalytic activity for methylene blue dye degradation," *Research Square*, PREPRINT (Version 2021) available at Research Square, 2023.